Journal of the European Ceramic Society

Reactive consolidation and high-temperature strength of the HfB2–SiB6 system.

--Manuscript Draft--

Manuscript Number:	JECESOC-D-21-02424R2
Article Type:	Full Length Article
Keywords:	hafnium diboride; reactive decomposition; silicon hexaboride; flexural strength; high-temperature materials.
Corresponding Author:	Dmytro Demirskyi, Ph.D. Tohoku Daigaku Sendai, JAPAN
First Author:	Dmytro Demirskyi, Ph.D.
Order of Authors:	Dmytro Demirskyi, Ph.D.
	Toshiyuki Nishimura
	Tohru Suzuki
	Kyosuke Yoshimi
	Oleg Vasylkiv
Abstract:	Reactive consolidation using HfB2–SiB6 powders resulted in a three-phase ceramic composite; i.e., HfB2, B12(C,Si,B)3 and SiC. Improvement in the hardness (24.5±0.7 GPa) can be attributed to the formation of the B12(C,Si,B)3 phase. Fracture toughness by indentation (6.8±2.4 MPa·m1/2), single-edge notched bend specimens (4.6±0.4 MPa·m1/2) and room-temperature strength (513±21 MPa) of the HfB2–SiB6 composite produced by spark plasma sintering was higher or on the same level as the HfB2–SiC ceramics. The high-temperature flexural strength tests suggested that the strength would decrease monotonically with an increase in temperature. At or below 1600 °C, only a linear stress-strain response was observed, and produced a mean strength of ~320 MPa. During the tests at 1800 °C, we observed a nonlinear deformation indicating ongoing plastic deformation which lead to the strength decrease down to 230±30 MPa.

Reactive consolidation and high-temperature strength of the HfB_2–SiB_6 system

Summary of Novel Conclusions

Decomposition of the silicon hexaboride takes place during the spark plasma sintering at 1900 °C. This decomposition results in the formation of the $B_{12}(C,Si,B)_3$ and cubic β-SiC. Spark-plasma consolidation using HfB_2–SiB_6 powders resulted in a three-phase ceramic composite; i.e., HfB_2, $B_{12}(C,Si,B)_3$ and SiC. This composite showed a good ratio between hardness (24.5±0.7 GPa) and toughness (4.6±0.4 MPa $m^{1/2}$). Improvement in the hardness can be attributed to the formation of the $B_{12}(C,Si,B)_3$ phase with a #166 *R*– *3 m* crystal structure and lattice parameters a = 5.60(7) Å and c = 12.15 Å. The high-temperature flexural strength tests suggested that this composite will show plasticity only at 1800°C.

Dear Editor of Journal of the European Ceramic Society Laura Silvestroni,

We would like to submit the revised version (R2) of the manuscript entitled "Reactive consolidation and high-temperature strength of the HfB_2–SiB_6 system" by Dmytro Demirskyi, Toshiyuki Nishimura, Tohru Suzuki, Kyosuke Yoshimi and Oleg Vasylkiv for publication in the Journal of European Ceramic Society.

First, the authors would like to express our gratitude to you, and reviewer(s), as we appreciate the feedback received during the review process helped us to improve the presentation of our results.
Second, we introduced the references on the ZrB_2, ZrB_2-based and HfB_2-SiC ceramics as suggested by the reviewer. Because, no particular link or suggestions were provided we screened data on these bulks for the last 10 years.
Third, we rearranged the manuscript, so the SiB_6-related specifics are introduced before the composite. We appreciate this suggestion. To explain the triagonal shape of the cubic-SiC grains we present **Figure 8** and two movies as supplementary video files.
Next, we cannot speculate on the strength/toughness values vs size used. We used one of the configurations suggested by the standard. Obviously, a different configuration may result in a slight deviation from the values we report. Nevertheless, in the case of the temperature dependence of strength, the size of the samples was the same, so one may expect the trend to be the same.
Finally, we cannot present the data (properties/XRD) on the SiB_6 content, as we continue to test the specimens, but the 30 vol.% SiB_6 showed the highest strength at room temperature.

Hopefully, the revised copy of this manuscript will look more satisfactory to the reviewer and to the future reader.

All authors have seen and approved the revised manuscript for submission to Journal of European Ceramic Society.

On behalf of authors,

Dmytro Demirskyi

Reactive consolidation and high-temperature strength of the HfB_2–SiB_6 system

D. Demirskyi (a,b,c)†, T. Nishimura (b), T.S. Suzuki (b), K. Yoshimi (c), O. Vasylkiv (b)†.

(a) WPI-Advanced Institute for Materials Research (WPI-AIMR), Tohoku University, 2-1-1 Katahira, Aoba-ku, Sendai, 980-8577 Japan
(b) National Institute for Materials Science, 1-2-1 Sengen, Tsukuba, Ibaraki 305-0047, Japan
(c) Department of Materials Science and Engineering, Tohoku University, 6-6-02 Aramaki Aza Aoba, Sendai, 980-8579, Japan

Abstract

Reactive consolidation using HfB_2–SiB_6 powders resulted in a three-phase ceramic composite; i.e., HfB_2, $B_{12}(C,Si,B)_3$ and SiC. Improvement in the hardness (24.5±0.7 GPa) can be attributed to the formation of the $B_{12}(C,Si,B)_3$ phase. Fracture toughness by indentation (6.8±2.4 MPa·$m^{1/2}$), single-edge notched bend specimens (4.6±0.4 MPa·$m^{1/2}$) and room-temperature strength (513±21 MPa) of the HfB_2–SiB_6 composite produced by spark plasma sintering was higher or on the same level as the HfB_2–SiC ceramics. The high-temperature flexural strength tests suggested that the strength would decrease monotonically with an increase in temperature. At or below 1600 °C, only a linear stress-strain response was observed, and produced a mean strength of ~320 MPa. During the tests at 1800 °C, we observed a nonlinear deformation indicating ongoing plastic deformation which lead to the strength decrease down to 230±30 MPa.

Keywords: hafnium diboride; reactive decomposition; silicon hexaboride; flexural strength; high-temperature materials.

† Authors to whom correspondence should be addressed, Dmytro Demirskyi, demirskyi.dmytro.e2@tohoku.ac.jp, Oleg Vasylkiv oleg.vasylkiv@nims.go.jp

1. Introduction

It is well established that ceramic composites of refractory diboride metals, such as ZrB_2 or HfB_2 with silicon carbide (SiC), have become a backbone for the ultra-high-temperature ceramics (UHTC) development [1–3]. Due to the initial success reported in [4], it is not surprising that the processing and characterization of ZrB_2–SiC is being widely reported by numerous groups [5–7]. Slightly less attention has been devoted to the HfB_2–SiC composites as the main issue for these ceramics is the relative density of the hafnium diboride [1]. Nevertheless, HfB_2−SiC composites have a higher resistance to ablation or oxidation than the ZrB_2–SiC composites [3, 8–10].

In terms of the engineering properties, the room and high temperature mechanical properties of the HfB_2–SiC composites have been reported in the literature [11–16]. In particular, Bellosi et al. [12] examined the mechanical properties of the HfB_2–SiC composites prepared via hot pressing and spark plasma sintering. The reported strengths were 590±50 MPa and 600±15 MPa at room temperature (RT) and at 1500 °C (in air), respectively. Zapata-Solvas et al. [13] prepared a HfB_2–20 vol% SiC ceramic using 2 wt% La_2O_3 by spark plasma sintering. The average strength was 690 MPa at RT, but decreased to 480 MPa at 1400 °C. More recently, Guo et al. [11] showed that the strength can remain unchanged at ~600 MPa between RT and 1600 °C. Below 1400 °C flexural strength for the HfB_2–SiC ceramics can be controlled by thermal stresses. These thermal residual stresses in ZrB_2–SiC composites were completely relaxed at ~1400 °C [17], thus any increase/decrease in strength above 1400 °C can be explained by the grain size of diboride and silicon carbide, ternary phases, loading rate or plasticity [18–30]. For instance, the increase in the strength can be attributed to the activation of the plastic flow in the composite as it facilitates the stress relief. A significant contribution of plasticity during the deformation might lead to the decrease in strength, especially

when the shape of the strain-stress curve changes from a linear with a plastic end to the typical plastic curve (sigmoidal strain-stress curve).

In addition, it is important to note that bulk HfB_2 has an average strength at 1600 °C [4,13,15,18]. Numerous results have indicated that thermal stresses, bonding and phase distribution between the metal diboride and silicon carbide play a dominant role in the high-temperature strength [4,11,17].

Alternatively, there were attempts to consolidate ZrB_2/HfB_2 using B_4C or SiB_6 sintering aids [31–33], as it is possible to achieve a 'superhardness' in the ZrB_2–SiC–B_4C system [34]. Ref. [32] suggests the improvement in the hardness of ceramic composites. However, the results in [33] indicate that SiB_6 disappears after sintering and only diboride can be detected by X-ray diffraction.

The present study aims to examine the HfB_2–SiB_6 as an alternative to the HfB_2–SiC approach. We propose the reactive decomposition of the silicon hexaboride as main method to produce a ceramic composite with a good balance between hardness, strength and toughness. In particular, we focused our attention on the flexural strength between room temperature and 1800 °C.

2 Materials and Methods

Commercially-available HfB_2 (Grade O, Lot #T302510, Japan New Metals Co., Ltd., Osaka, Japan) and SiB_6 (Lot #348108, International Lab, USA) were used as the starting materials. The concentration of the secondary elements in the HfB_2 powder was as follows: Fe 90 ppm, Nb ≤ 200 ppm, Zr ≤ 120 ppm, C< 0.5 wt.%, N ≤ 0.5 wt.%, and O <0.7 wt.%. For SiB_6 the main impurities were Na 100 ppm, Mg ≤ 100 ppm, Al ~ 0.1 wt.%, and O ~ 0.1 wt.%. SiB_6 had the following chemical composition 70±1.0 wt.% B, 30±1 wt.% Si, free silicon ≤ 0.1 wt.%, carbon ≤ 0.2 wt.%.

These commercial powders were used for consolidation by the spark plasma sintering (SPS) method at a 80:20 vol.% ratio between HfB_2 and SiB_6. Powders were mixed using the Intelli-Mixer RM-2M (ELMI, Latvia) mixer (*see Suppl. Data Video1*). This procedure excludes using solvents or grinding the materials. The mixing process and partial crushing of ceramic particles occur due to fast vibrations in the relatively small volume (50 ml). After this mixing, powders were inserted into the SPS graphite die. Unless stated otherwise, we used an inner Ta-foil (Sigma-Aldrich Chemie, 0.025 mm thick, 99.9+% metal basis) and outer graphite foil configuration, in which the Ta-foil would be in direct contact with the powder. From the top/bottom of the specimen, the Ta-foil would be followed by the graphite circle. When we need to distinguish the bottom side, Nb foil (Sigma-Aldrich Chemie, 0.025 mm thick, 99.9+% metal basis) + graphite foil configuration was used. These steps were made to minimize the diffusion of carbon [35,36] into the powder mixture during the SPS process. The SPS experiments were conducted using the 'Dr. Sinter' 1050 (Sumitomo, Japan) unit with a 25-mm die, and typically, 20 to 26 g batches were produced.

The schedule for the HfB_2–SiB_6 specimens prepared in this study had four major steps: (1) heating to 700 °C in four minutes followed by (2) a 100 °C/min heating to the densification temperature of 1900 °C. At 1900 °C, then a dwell of 10 min was used as a homogenizing step. The final step included cooling to 600 °C in 40 minutes. The pressure of 32 kN was maintained during the consolidation and cooling stages. Argon gas at the flow rate of 2 L/min was used.

Furthermore, we performed model experiments on the monolithic SiB_6. We performed the SPS of SiB_6 at 1900 °C using identical heating and cooling stages, but without any dwell. These SPS experiments were performed using a Ta/Nb protection. In addition, we performed experiments using graphite foil, which is

considered as a ‘regular’ configuration in a majority of studies using spark plasma sintering.

An X-ray diffraction (XRD) analysis (D8 Advance, Bruker, Karlsruhe, Germany) was performed on the diamond-polished surfaces using Cu-Kα radiation. The intensity data were collected over the 2θ range of 15°–145° in steps of 0.02° using a sampling time of 10 s for each step. The software used for refinement was TOPAS (TOPAS Ver. 4.2, Bruker AXS, Germany). Instrumental broadening was determined using a NIST 660b LaB_6 standard run under the same conditions for each ceramic sample.

The structural characteristics of the composite ceramics were studied by scanning electron microscopy (SEM, JCM-6000, JEOL) using secondary (SE) or backscattered electrons (BSE mode). The Energy-dispersive X-ray spectroscopy analysis (EDX) was performed using a JEOL DX200s analyzer.

The three-point flexural strength was determined using rectangular blocks (1.5×2×25 mm, ASTM C1211−13, configuration A) and the strength testing equipment that was previously reported in [37]. The three-point flexural strength tests were conducted using Shimadzu AG-X plus (Shimadzu, Japan) equipped with a specially designed high-temperature enclosure (NEMS, Japan) housing W heating elements and capable of temperatures up to 2000 °C. This enclosure allows to measure up to 12 specimens in a single load as it uses a carousel (roundabout) scheme to rotate and interchange specimens. The temperature inside the hot zone was controlled by two thermocouples and an IR pyrometer. The pyrometer was used to control of temperatures above 1800 °C. The vacuum space was pumped to $4 \cdot 10^{-3}$ Pa and backfilled with high-purity argon at least 3 times for the high-temperature tests. Argon had a purity 5.0. The main impurities were $O_2 \leq 2$, $N_2 \leq 5$, $H_2O \leq 3$, and C_nH_m (such as methane) ≤ 0.2 in ppm. In the case of measurements in a vacuum, the heating sequence could not be initiated if a vacuum was above $5 \cdot 10^{-3}$ Pa.

A span of 16 mm was used. Measurements were performed using with a loading speed of 0.5 mm/min.

The fracture toughness of the ceramics was evaluated by specimen bending testing which contained a single-edge notch (SENB method) following ASTM C1421–10. The toughness was tested in the same direction as the pressure was applied during the SPS consolidation. Details of the testing configuration and the notch profile were presented in ref. [38]. The fracture toughness data were averaged based on three tests.

For the high-temperature flexural strength tests, the following heating schedule was used: from room temperature to 200 °C in 10 minutes and from 200 °C to the testing temperature at a rate of 18 °C/min. A dwell time of 5 minutes was employed before the flexural test at the testing temperature. For the tests at 1800 °C, specimens were gradually cooled and heated up to the test temperature with a rate of 12 °C/min from 1570 °C [39]. During these heating and cooling procedures, the specimen was kept 20 mm below the hot zone used for the tests. For the tests conducted below 1600 °C the specimen was lowered in 5 minutes for exchange without any dwell at the temperature of the test. After testing at temperature below or equal to 1600 °C, cooling from the testing temperature to room temperature was performed at a rate of 20 °C/min. The flexural strength data were averaged based on four tests at the elevated temperature and by five tests at room temperature. Specimens were also tested in a vacuum and in nitrogen. Four tests were performed at 1200 °C, 1600 °C and at 1800 °C.

The hardness was determined by an MMT-7 Vickers hardness tester (Matsuzawa MMT-7; Matsuzawa SEIKI Co., Ltd., Tokyo, Japan) using loads of 9.8 N and 98 N with a dwell time of 15 s following the standard procedure (ASTM C 1327–15). The indentation toughness of the selected specimens was evaluated using indents after 98 N loads and by the procedure proposed by Anstis et al. [40].

The hardness and the indentation fracture toughness were the average of at least 12 measurements.

3. Results and discussion

3.1. Reactive decomposition of bulk SiB_6

In order to address the decomposition of the silicon hexaboride during the SPS processing of the HfB_2–SiB_6 ceramics, we performed model experiments on the monolithic SiB_6. Similarly, we performed the SPS of the SiB_6 at 1900 °C using identical heating and cooling stages, but without any dwell. **Figure 1** shows the microstructure of the SiB_6 after decomposition at 1900 °C. The illustration of the SPS process which involves tantalum foil and graphite foil is presented in (**Fig. 1** (c)). As a rule the 30-μm thick tantalum carbide foil originated from the SPS process (see ref [41] for the SEM of this foil).

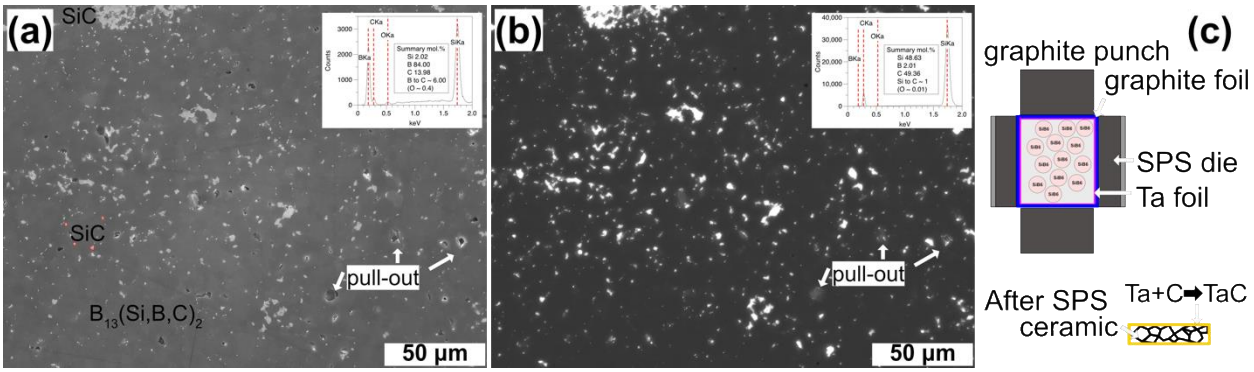

Figure 1. Microstructure of the SPSed SiB_6 ceramic after consolidation at 1900°C using a Ta-foil. The volume fraction of the SiC clusters using Fiji was 4.6±0.3 vol.%. (a) was obtained in the SE mode, (b) was obtained in the BSE mode. Light-gray phases in (b) are due to the grain pull-outs. Insets in (a) and (b) provide typical EDX for the $B_{13}(Si,B,C)_2$ and SiC phases, respectively. (c) illustrates how Ta-foil was used during the SPS process: reaction between tantalum foil and graphite foil produces the ~30 μm thick TaC layer (see ref. [41] for details).

An XRD analysis (**Figure 2**) suggested that a three-phase ceramic was formed. Graphite, cubic silicon carbide and boron carbide with the structure $B_{13}C_2$ were identified using the Rietveld refinement. In this case, the lattice parameters for the boron carbide phase were a = 5.58 Å and c = 12.25 Å. We may emphasize that the initial silicon hexaboride powder was close to stoichiometric. The refinement in **Figure 3** yielded the following lattice parameters for the *Pnnm* SiB_6 structure: a = 14.42 Å, b = 18.30 Å, and c = 9.89 Å. These are in the good agreement with Vlasse et al. [42] of a = 14.39 Å, b = 18.31 Å, and c = 9.91 Å.

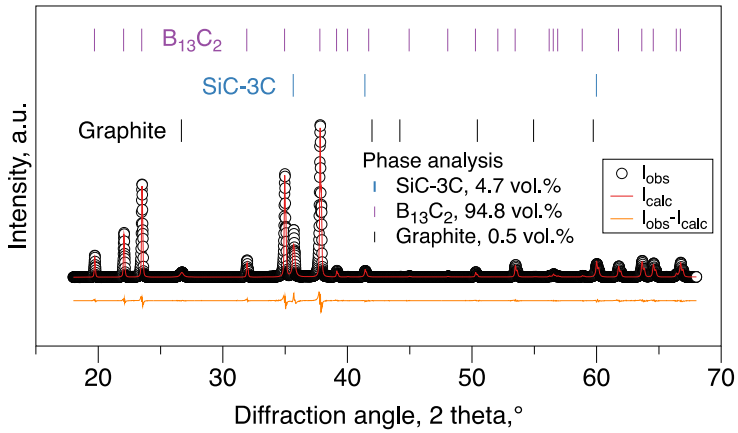

Figure 2. Observed and refined X-ray diffraction pattern of the SiB_6 after SPS at 1900 °C. Vertical lines show the Bragg peak positions for the refined phases. The lattice parameters for the $B_{13}C_2$ phase are a = 5.58 Å and c = 12.25 Å.

The majority of the possible reactions were discussed by Telle et al. [43,44]. Below 2000 °C, SiB_6 should decompose into a Si liquid and SiB_n-type phase (n = 12–24). The latter phase is expected to decompose into β-boron and a liquid at 2060 °C [44]. Considering the results of the SEM and XRD data, the reaction between the carbon and silicon hexaboride can be summarized as follows:

$2\ SiB_6 + 5\ C = 3\ B_4C + 2\ SiC$

Of course, in the view that a more complex $B_{12}(C,Si,B)_3$ phase is being formed one can rearrange this reaction as:

$SiC + 5\ C + 5\ SiB_6 = 2\ B_{12}(CSiB)_3$.

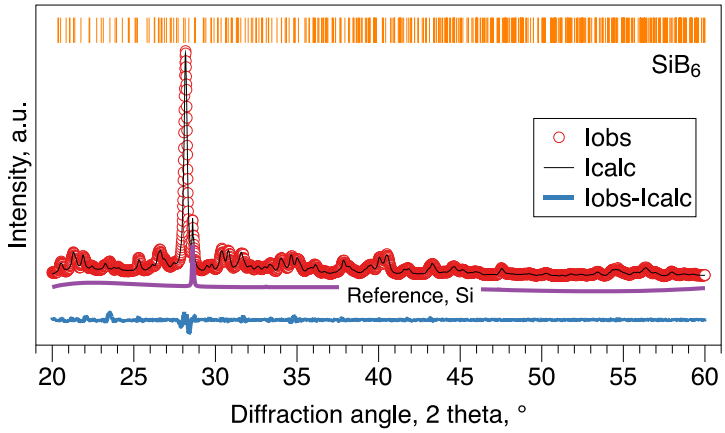

Figure 3. X-ray diffraction pattern of the raw SiB_6 powder. Silicon was used as an external standard. All other peaks belong to silicon hexaboride. The vertical lines show the Bragg peak positions for the SiB_6 phase. The lattice parameters for the SiB_6 phase (space group #58, *Pnnm*) are a = 14.42 Å , b = 18.30 Å and c = 9.89 Å .

Here one should bear in mind that for the formation of 0.1 mole of $B_{12}(CSiB)_3$, it is necessary to use 0.25 moles of SiB_6 and C (23.2g and 3.0 g, respectively). Obviously, such an estimation is valid for the stoichiometric $B_{12}(CSiB)_3$. SiC should form as well, which requires an additional amount of carbon. The B balance could not be performed as well, as B or B_4C is known to react with oxide to form diborides [45–47]. One can show, that at 1900 °C reaction involving hafnium oxide with boron/boron carbide will have negative Gibbs energy (~ -125 kJ/mole using data from [48,49]), indicating that reaction is highly favorable.

The total amount of carbon transferred to the powder system during the SPS is currently unknown. In order to illustrate the protective nature of the tantalum foil, we performed experiments only using graphite foil. **Figure 4** shows the

microstructure of the SiB_6 consolidated at 1900 °C without the tantalum foil. Even after polishing off top two mm of the sample, we can still identify up to 8 vol.% of graphite. Nevertheless, the total amount of silicon carbide was on the same level as for the specimen SPSed using a tantalum foil.

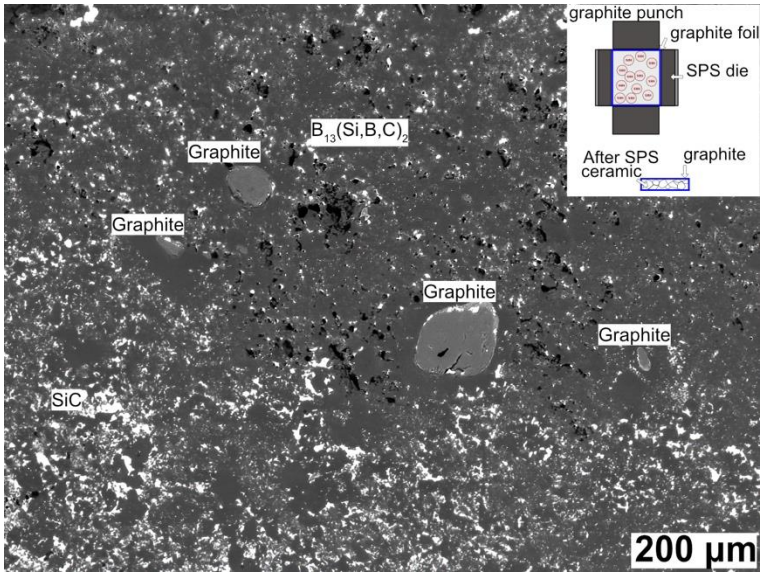

Figure 4. Microstructure of the SiB_6 ceramic after SPS at 1900 °C. Powders were consolidated using a 'regular' SPS packaging (see inset), which involves only graphite foil. The thickness for such foil is ~1 mm. Top two millimeters was removed during polishing. The volume fraction of the SiC clusters using Fiji was 5.1±0.4 vol.%. The graphite clusters (medium-gray color) occupied 6.2±0.2 vol.%.

3.2. Reactive consolidation of a HfB_2-SiB_6 mixture by SPS

Using SiB_6 during the consolidation of the HfB_2-based ceramic results in a reaction between the silicon hexaboride and carbon that comes inwards from the graphite felt during the SPS. The majority of the possible decomposition reaction were discussed by Telle et al. [43,44]. Below 2000 °C, SiB_6 should decompose into a Si liquid and SiB_n-type phase (n = 12–24), which decomposes into β-boron and a liquid at 2060 °C [43]. In this case, the carbon diffusion may lead to the formation of the boron carbide as was observed for the TiB_2–B mixture [50].

When analyzing the shrinkage of the HfB_2–SiB_6 powder mixture, one can divide a shrinkage profile above 1600°C into four zones. Below 1800 °C the powder mixture slowly densifies. Between 1800 °C and 1815 °C, and at dwell of 1900 °C (**Figure 5**) there was an increase in the shrinkage rate. The first temperature interval for rapid shrinkage is in close proximity with the observation of [51] for liquid phase formation and it is attributable to the decomposition of the SiB_6 into boron and silicon and presumably a liquid (hence rapid shrinkage).

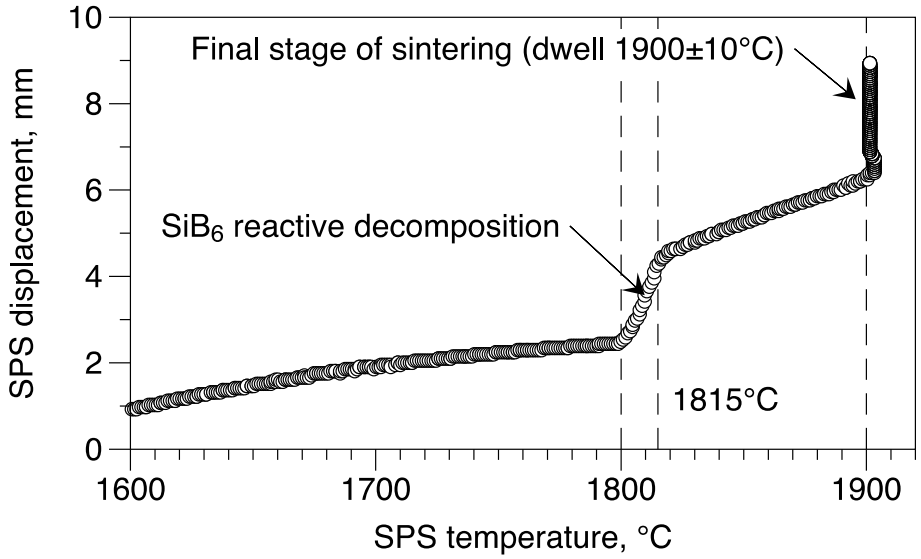

Figure 5. Shrinkage curve of the HfB_2–SiB_6 composite during spark plasma sintering at 1900 °C.

Figure 6 shows that after reactive consolidation of the HfB_2–SiB_6 powder mixture one can identify a two-phase ceramic composite. Such a composite includes the HfB_2 and B_4C-type phase. Similar to the findings in [43], we defined this phase as $B_{12}(C,Si,B)_3$. The Rietveld refinement indicated the ratio of 72:28 vol.% between HfB_2 and $B_{12}(C,Si,B)_3$. We used the following structure cif files from the NIMS database [52]: $B_{13}C_2$ # 4296467450 citing [53], HfB_2 # 4295219124 citing [54].

Following a report by Telle [43] we refined the structure assuming that the Si substitutes the C in the Wykoff *c* position in the *R-3m* crystal cell.

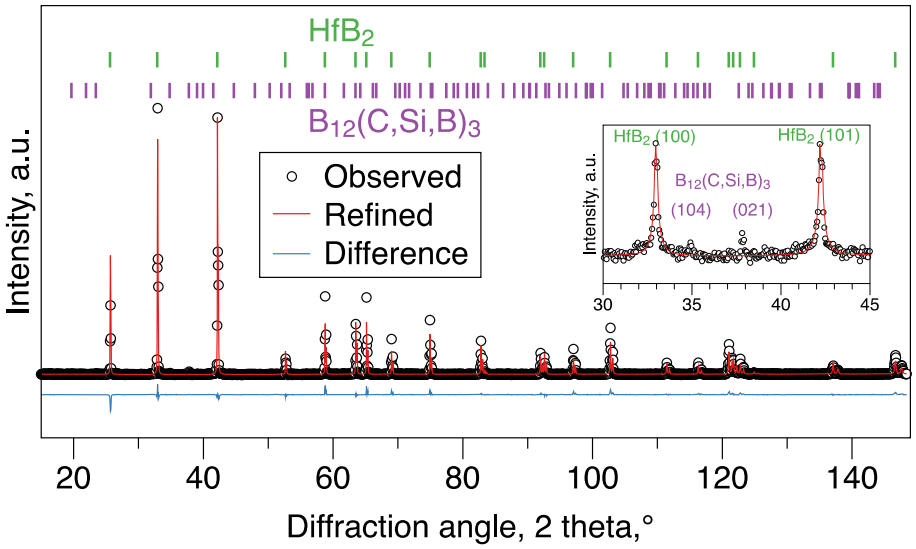

Figure 6. Observed and refined X-ray diffraction pattern of the HfB_2–SiB_6 ceramics after SPS. Inset shows position of the most intensive peaks of the $B_{12}(C,Si,B)_3$ phase on a logarithmic scale. The lattice parameters for the $B_{12}(C,Si,B)_3$ phase are a = 5.60(7) Å , and c = 12.15 Å . The Bragg peak positions for HfB_2 and $B_{12}(C,Si,B)_3$ are indicated by the green and violet vertical markers, respectively.

This ratio between phases was confirmed by SEM observation using ImageJ/Fiji software (U.S. National Institutes of Health, MD, USA) (see **Table 1** [55–59]). In addition to the HfB_2 and $B_{12}(C,Si,B)_3$ phases we also observed at least 1 % SiC by SEM. A histogram (not shown) for the SiC area using a multiple SEM images showed that the mean value for the SiC content was 2.2 vol. %. One can see that there is a close proximity in the volume fractions observed for the $B_{12}(C,Si,B)_3$–SiC clusters with a pseudo-eutectic structure (**Figure 7**) when compared to with data for B_4C–SiC eutectics reported in [58,59]. Local formation of the ternary eutectic is

unlikely as it would require temperatures exceeding 2000 °C–2100 °C [59] and a different ratio between components.

In some particular instances (see **Figure 7**), the large clusters of the $B_{12}(C,Si,B)_3$ included up to 20 vol.% SiC. In such instances these 100–200 μm aggregates had a pseudo-eutectic structure, as the SiC inclusions were triagonal and needle-shaped crystals. The inset in **Fig. 7 (b)** shows the typical microstructure of the SiC–B_4C eutectic obtained by the β-SiC and B_4C mixture and SPS processing at 2085±10°C using the approach presented in [51]. In some cases, the $B_{12}(C,Si,B)_3$ clusters had the shape of a compressed disk and this shape is believed to originate due to the pressure used during the SPS.

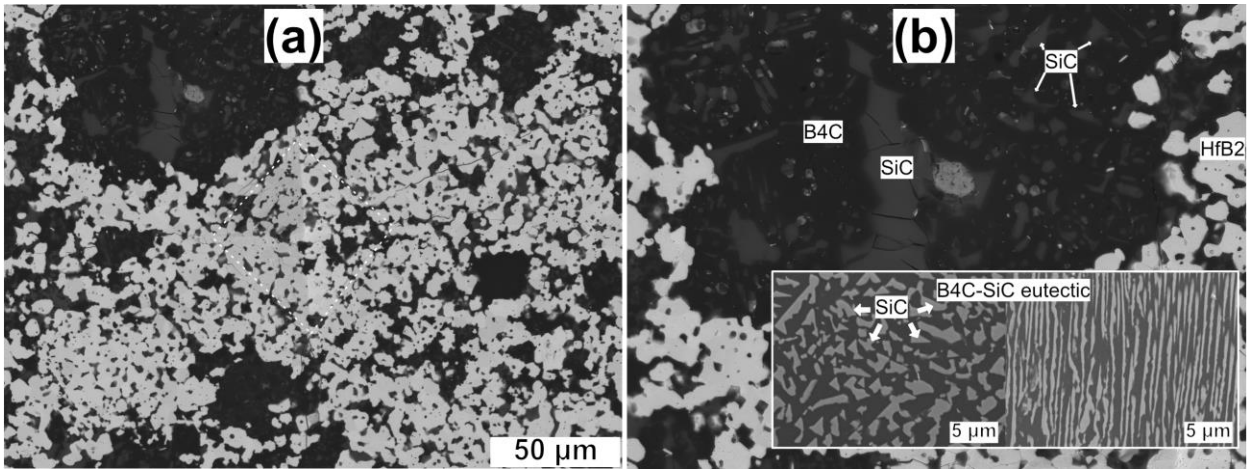

Figure 7. Microstructure of the HfB_2–SiB_6 ceramic SPSed at 1900 °C in the vicinity of the pseudo-eutectic aggregate. (b) shows the enlarged area of the $B_{12}(C,Si,B)_3$–SiC area. The crack in the SiC phase here originated from the indent by the load of 98 N. Inset in (b) shows typical B_4C–SiC eutectic structures prepared as parallel experiment using the SPS method with the 75 B_4C:25 SiC vol.%. The maximum shrinkage rate indicating the eutectic formation as in [51] during the SPS of the B_4C–SiC eutectic was 2085±10°C.

The formation of triagonal and needle-shaped β-SiC crystals can be explained by its growth habit. According to [60] (111) and (220) are the fastest growing planes, while the (111) has been suggested as the lowest energy plane [61,62]. While, Nishiguchi et al. proved experimentally the (220) plane possesses the lowest surface formation energy in β-SiC [63].

The process for the evolution of the surface during the crystal growth can be visually predicted using CrystalGrower [64]. The crystallographic data were used from COD # 1010995, and the energy used for the calculation was 550 kJ/mol as an activation energy from ref. [65] for the creep of SiC. The results of the numerical simulation of the growth process for SiC are presented in **Fig. 8** using Ovito [66] (*see Suppl. Data Video2, Video3* for details). One can see the formation of the step-like triagonal surfaces, which in the case of the simulation is directly connected to the surface diffusion during the crystal growth.

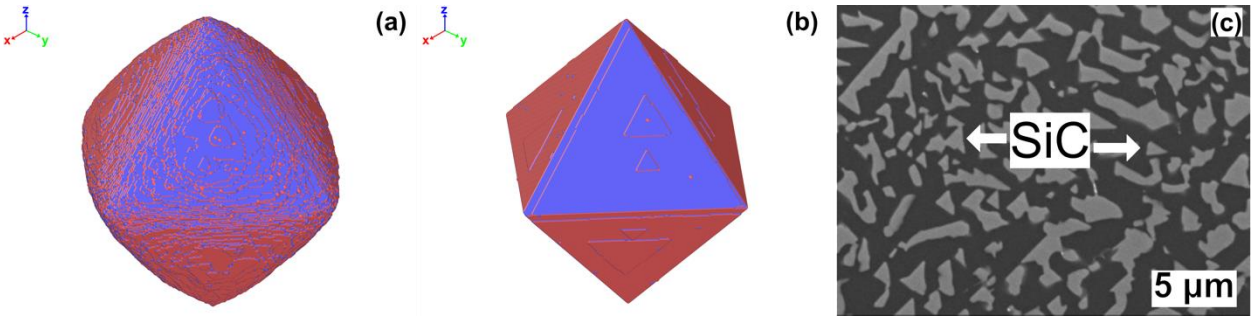

Figure 8. Illustration of the surface during the crystal growth process for cubic silicon carbide at (a) 1900 °C and (b) 1000 °C. (c) shows typical B_4C–SiC eutectic structure.

This brings up the question on the fairly large amount of carbon required to completely transform β-B presumably formed during the SiB_6 decomposition and also on the amount of Si-liquid that presumably vanished during the SPS consolidation. For pure silicon, the boiling point is rather high (3265 °C), while the silicon oxides such as SiO_2 or SiO were not detected by XRD or SEM. For this

reason, we believe that the majority of the silicon would naturally dissolve in the $B_{12}(C,Si,B)_3$ phase. As noted in [44], the formation of the $B_{12}(C,Si,B)_3$ solid-solution is accompanied by the formation of the cubic β-SiC which melts with SiB_6 and the residual Si above 1380 °C. Considering the visual similarity in the shape of the β-SiC and B_4C eutectic (**Figs. 7,8**) and pseudo-eutectic clusters in the HfB_2–SiB_6 composite after consolidation, the predominant contribution of the Si into the $B_{12}(C,Si,B)_3$ solid-solution is highly probable.

According to analysis of Telle et al. [43], the lowest experimental and calculated temperature for the $SiB_6 \leftrightarrow SiB_n$ + liquid, where n = 12–14 … 23, was 1850 °C, while several experimental works reported the temperature of between 1898 °C and 1989 °C [43]. That being said, it is important to note that the ternary Si–B–C system features an eutectic formation that may require additional clarification.

First, as the Si incorporation into the boron carbide lattice always results in the release of C or the simultaneous formation of SiC, if Si is present in excess, it was concluded that Si substitutes for C assuming that there is no carbon in the boron carbide on the interstitial sites [44].

Second, the formation of a solid solution of $B_{12}(B,C,Si)_3$ is accompanied by the precipitation of cubic β-SiC which eutectically melts with SiB_6 and the residual Si above 1380 °C [43].

Finally, according to [67], transformation of the cubic β-SiC into hexagonal polytypes can be expected after a lengthy dwell at elevated temperatures. Considering that the XRD of the reference SiB_6 (*see section 3.1*) resulted only in cubic silicon carbide, one can dismiss the idea of a local overheating during the SPS dwell. However, of course, it is still possible and highly probable, but the overall magnitude of the temperature difference is unlikely to be higher than 100 °C. Alternatively, the SiB_6–SiC eutectic was initially formed, then the silicon hexaboride

decomposition yielded local quasi-eutectic $B_{12}(B,C,Si)_3$–SiC clusters. EDX -probing (**Figs. 9,10**) suggested that boron carbide phase may contain up to 5.4 mol.% of Si. According to Telle [43] the maximum solid solubility of Si in boron carbide lattice is 2.5 ± 0.3 mol.% at 2050 °C. While [68] and [69] reported solubility of 6 mol.% and 1.8 mol.%, respectively.

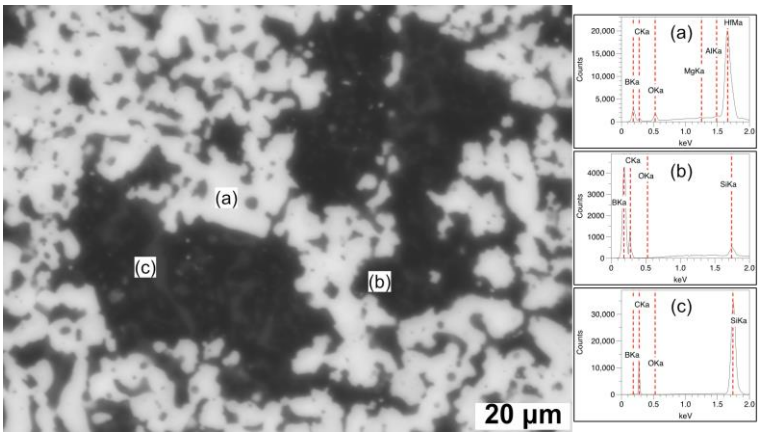

Figure 9. SEM micrographs of HfB_2-SiB_6 ceramics consolidated using the spark plasma method. Pale-gray phase is hafnium diboride, while the dark black is the Si-rich boron carbide phase. Light-gray phase was identified as silicon carbide. (a)–(c) contain EDX data from the spot analysis.

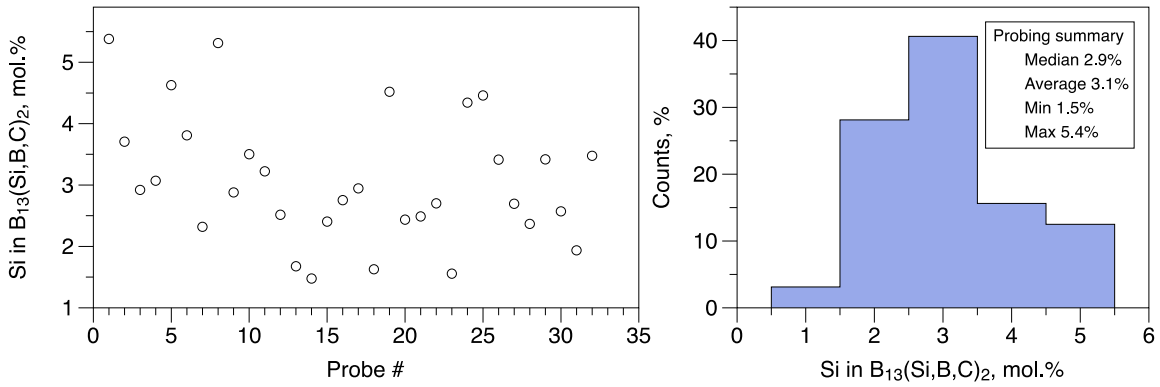

Figure 10. Silicon content for the $B_{13}(Si,B,C)_2$ as detected by the EDX analysis performed on the polished surfaces of the SPSed HfB_2–SiB_6 composite. Right image shows a distribution frequency of Si content in the $B_{13}(Si,B,C)_2$.

Carrasco-Pena et al. [33] could not identify the SiB_6 peaks or any secondary peaks after the SPS of ZrB_2–SiB_6 at 1750 °C. The XRD revealed only peaks of ZrB_2, while the SEM analysis suggested the presence of the fairly large aggregates of the some Si/B phase with an average grain size of ~2 μm. Furthermore, authors in [33] tentatively identified the $Si_{11}B_{31}$ phase in the composite; however, there were some unidentified weak X-ray peaks.

3.3. Mechanical performance of HfB_2-SiB_6 ceramics

For the ZrB_2–SiC–B_4C ceramics [34] one can observe the regular hardness 20±1 GPa or 'superhard' 28.9±1.6 GPa using a 9.8 N load. These values were similar to those measured for nominally pure ZrB_2 (23 GPa) or ZrB_2–SiC (24 GPa) [34]. The hardness of the initially batched HfB_2–20vol.% SiB_6, resulting in a HfB_2–2.2 vol.%SiC– 23.3 vol.% $B_{12}(C,Si,B)_3$ (see **Table 1**) after the sintering, was 24.5±0.7 GPa using a 98 N load and 25.5±1.3 GPa using a 9.8 N. It is expected that the addition of the boron carbide yields higher hardness. The hardness of the HfB_2–B_4C ceramics was previously reported by Zou et al. for the 2 wt.% B_4C (8 vol.% B_4C) composite as 19.5 GPa [32]. Ordany'an and Dmitriev [56] reported a microhardness of 32.15 GPa for the eutectic HfB_2–B_4C ceramic composite (i.e., 82 vol.% B_4C) using a 100 gf load. The hardness of the B_4C-8 vol.% HfB_2 ceramics was 28.3±1.1 GPa [70]. Monolithic hafnium diboride showed a hardness of 19.8±0.7 GPa according to Zapata-Solvas et al. [13], while the HfB_2–20 vol.% SiC ceramics prepared within the same study had a 27.0±0.6 GPa hardness, which is on the same level with data for the present HfB_2–SiB_6 ceramic.

The fracture toughness of the HfB_2–SiB_6 composite was evaluated by the indentation method and by the flexural test at room temperature (**Fig. 11**). The indentation method using a 98 N load resulted in a broad range of values, and the mean toughness was measured to be 6.8±2.4 MPa $m^{1/2}$. The flexural approach

resulted in a toughness of 4.6±0.4 MPa $m^{1/2}$ using three specimens with size (3 mm×4 mm×25 mm, notch width 90 μm, depth 0.4–0.6 mm, a/W <0.15). However, during a typical fracture we noted that the load-displacement curve displayed several humps observed before the final fracture. The lowest peaks probably correspond to the $B_{12}(C,Si,B)_3$ aggregates as the typical fracture toughness for boron carbide lies within 2–3 MPa $m^{1/2}$ [71]. For reference, the 'superhard' ZrB_2–SiC–B_4C had a toughness of 3.1±0.6 MPa $m^{1/2}$[34]. Overall, the toughness measured by flexure is in good agreement with the toughness for the HfB_2 (3.3±0.4 MPa $m^{1/2}$) or HfB_2–20 vol.% SiC (5.0±0.4 MPa $m^{1/2}$) ceramics [13].

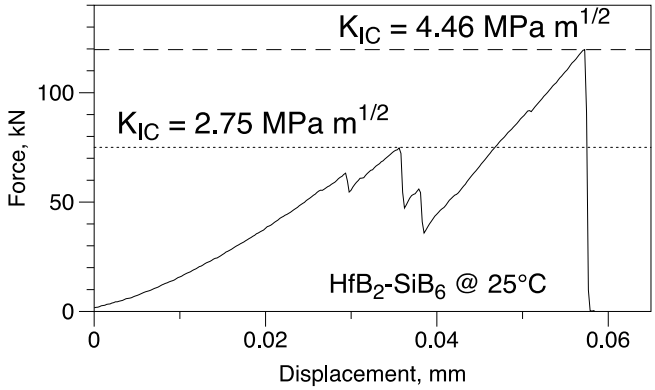

Figure 11. Force-displacement curve recorded during the fracture toughness evaluation using the single edge notched beam flexural test at room temperature.

The room-temperature strength of the HfB_2–SiB_6 composite was relatively high (513±21 MPa), i.e., slightly higher than 450–500 MPa expected for the monolithic hafnium diboride [4,13]. A considerable variation in the strength can be expected, significantly related with the size of the specimens. Within this study, we used the configuration A (1.5×2×25 mm) and configuration B (3×4×45 mm) should be tested in the future studies. With an increase in the temperature, the flexural strength decreased to 236±20 MPa at 1800 °C (**Figure 12**) [4,11,14–16]. In order to illustrate such a trend, the strength is presented on a logarithmic scale. The testing

medium had no real impact on the flexural strength as only a real deviation was observed when comparing the strength for the HfB_2–SiB_6 composite tested in nitrogen (red circle) and argon (black circle). A vacuum was used up to 1600 °C, and at this temperature, the data for all the collected specimens were not influenced by the medium for testing and lied within 315±25 MPa. The loading curves (**Figure 13**) suggests a significant contribution of plastic deformation to fracture as a visible deviation from linearity was observed.

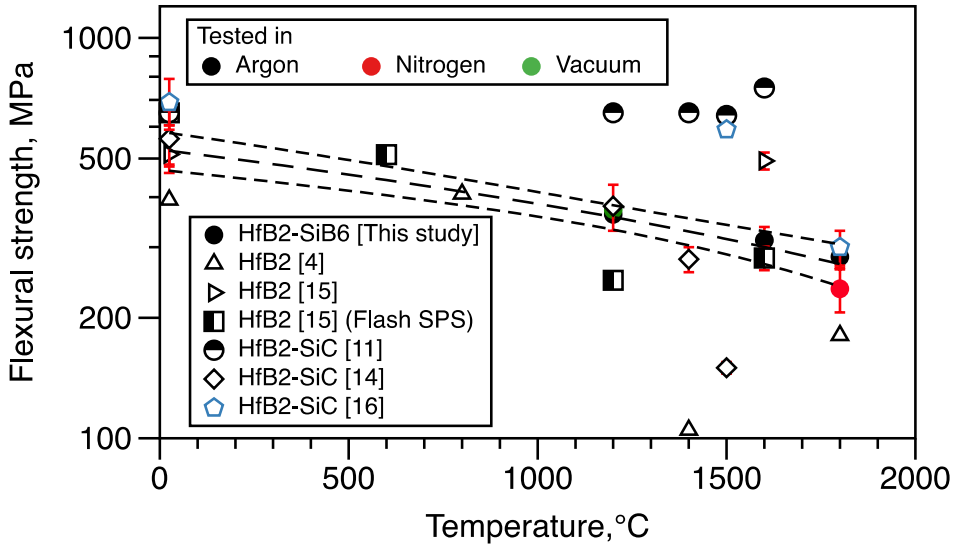

Figure 12. Effect of temperature and composition on the flexural strength of HfB_2-based ceramics [4, 11, 14–16]. Strength of 'as sintered' ceramic reported from ref. [16], and its corresponding test at 1500 °C was performed in air.

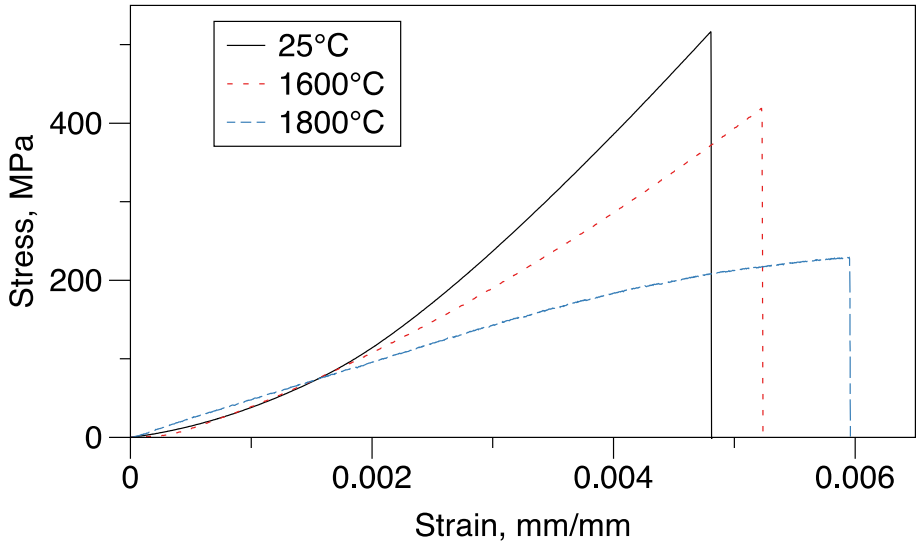

Figure 13. Typical strain-stress curves during flexural tests at 25°C, 1600°C and 1800°C.

Typical data previously reported for the monolithic HfB_2 and HfB_2–SiC ceramics show that, as a rule, these ceramics might have a decrease in strength at 1000–1200 °C due to the relaxation of thermal stresses accumulated during their high-temperature processing. An exception would be the data by Guo et al. [11] when the HfB_2–20 vol.% SiC (with B_4C and C additives) ceramic composite showed no change in its strength. At or below 1500 °C, only a linear stress–strain response was observed. At 1600 °C, however, the initial linear response was followed by a nonlinear deformation behavior. The increase in strength observed at 1600 °C was associated with a strong intergranular bonding, plasticity as plastic flow in the composite as it facilitates the stress relief; or as a result of the strengthening effects on the grain boundary phase at a high temperature [11].

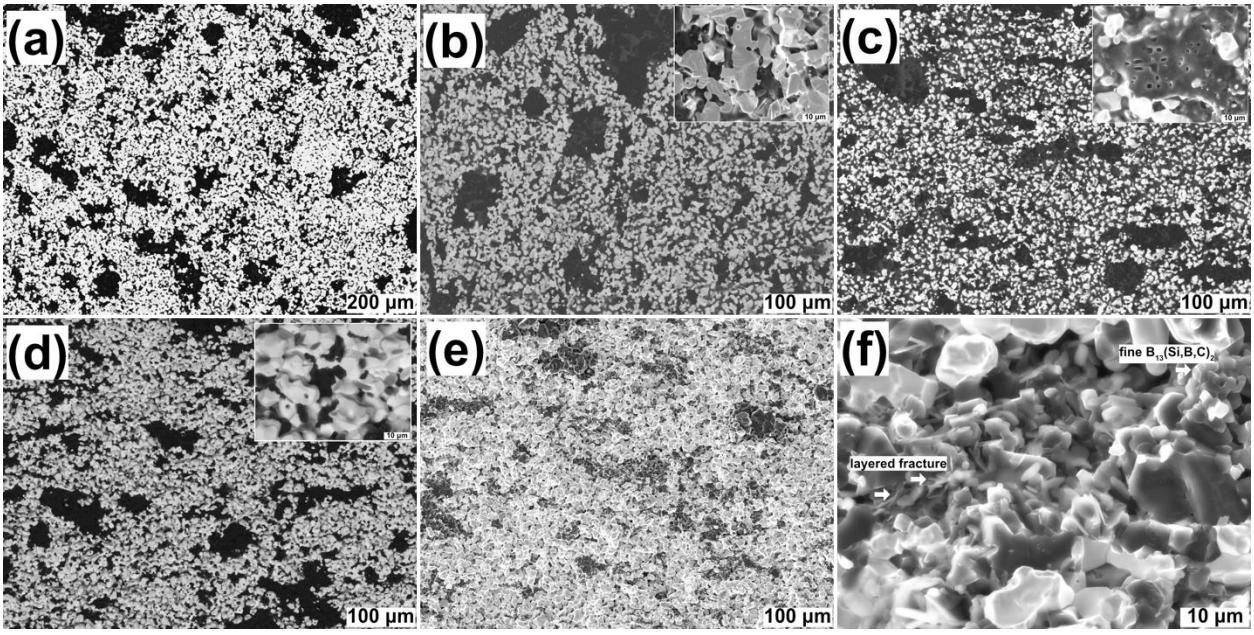

Figure 14. Representative microstructures of the HfB_2–SiB_6 ceramics. (a) polished, (b) fractured at room temperature, (c) fractured at 1600 °C, (d–f) fractured at 1800 °C. (e and f) taken in the SE mode. (a–d) were obtained in the BSE mode. (c,d) were tested in argon, while (e,f) were tested in nitrogen. In (f) a quasi-layered fracture was observed.

Data obtained for the HfB_2–SiB_6 composite essentially follow a trend typical for the monolithic hafnium diboride. We observed (**Fig. 14**) that an increase in the temperature does not change the predominant fracture mechanism as a mixed transgranular / intergranular fracture was observed at RT to 1800 °C. However, testing in nitrogen resulted in a more pronounced faceting of the HfB_2 or $B_{12}(C,Si,B)_3$ grains and in some instances (**Figure 14 (f)**) a quasi-layered fracture was observed. Inset in **Fig 14 (c)**, illustrates that $B_{12}(CSiB)_3$ phase is featured by intragranular pores, observed specifically for boron carbide. According to ref. [72] these pores in boron carbide are formed during extensive deformation from plastic flow and partly from sintering diffusion to conform with neighboring particles,

required extensive shear deformation which was accommodated by formation of these internal cavities.

Comparing these data with the study of Guo et al. [11], one may notice a substantial difference in the grain sizes (1 μm vs 10 μm). According to [73] for the coarser grains the possibility of grain-sliding is higher. By grain boundary sliding, stress concentrations retarding failure, thus allowing higher stresses to be reached before fracture. Grain boundary sliding is one of the dominant mechanisms for creep to occur. Because of a larger amount of the grain boundary area in fine-grained material the contribution to the creep deformation from grain boundary sliding will be higher in comparison to coarse-grained material [74].

Next steps in the ongoing research include preparing, optimizing and evaluating the high-temperature properties of Si-rich boron carbide–silicon carbide composites that can be prepared using silicon hexaboride decomposition. We will continue to study the reactive decomposition of HfB_2–SiB_6, since it is necessary to clarify the optimal content of SiB_6 and to evaluate the high-temperature toughness. It can be expected that additional flexural tests performed using specimens with a different configuration may provide further clarification of the reproducibility of the data presented in this study.

Conclusions

Several conclusions can be drawn from the present study. First, it was observed that high-temperature decomposition of the silicon hexaboride takes place during the spark plasma sintering at 1900 °C. Such a decomposition results in the formation of the $B_{12}(C,Si,B)_3$ and cubic β-SiC.

Second, decomposition promoted the formation of quasi-eutectic clusters, i.e. silicon carbide inclusions that had a peculiar triangular shape. The volume ratio between

the boron carbide and silicon carbide is 80 to 20 in vol.% in agreement with data reported for the $SiC - B_4C$ eutectic. Previous studies have suggested that the formation of the $B_{12}(C,Si,B)_3$ solid-solution from SiB_6 source is accompanied by the formation of β-SiC which melts with residual SiB_6 and Si above 1380 °C. Hence, it is highly likely that the formation of quasi-eutectic clusters follows a number of reactions involving liquid silicon and carbon from the graphite felt used during the SPS.

Next, reactive consolidation using HfB_2–30 vol.% SiB_6 powders resulted in a three-phase ceramic composite with a good ratio between hardness (24.5±0.7 GPa), toughness (4.6±0.4 MPa $m^{1/2}$) and room-temperature strength (513±21 MPa). Improvement in the hardness can be attributed to the formation of the $B_{12}(C,Si,B)_3$ phase with a #166 *R– 3 m* crystal structure and lattice parameters a = 5.60(7) Å and c = 12.15 Å, as estimated by Rietveld's refinement.

Finally, the high-temperature flexural strength tests on the HfB_2–SiB_6 ceramic, resulting in HfB_2–2.2 vol.%SiC– 23.3 vol.% $B_{12}(C,Si,B)_3$ after sintering, suggested that the strength would monotonically decrease with the increase in temperature. We found that this ceramic shows a macroscopic plasticity only at 1800°C. At 1600 °C, the strength measured using argon, nitrogen and vacuum was 315±25 MPa and the load-displacement remained linear up to fracture.

References

[1] W.G. Fahrenholtz, G.E. Hilmas, I.G. Talmy, and J.A. Zaykoski, Refractory Diborides of Zirconium and Hafnium, J. Am. Ceram. Soc., 95[5] (2007) 1347–1364. doi: https://doi.org/10.1111/j.1551-2916.2007.01583.x.

[2] E.W. Neuman, G.E. Hilmas, W.G. Fahrenholtz, Elevated Temperature Strength Enhancement of ZrB2–30 vol% SiC Ceramics by Postsintering Thermal Annealing, J. Am. Ceram. Soc., 99[3] (2016) 692–670. doi: https://doi.org/10.1111/jace.14029.

[3] E. Wuchina, E. Opila, M. Opeka, W. Fahrenholtz, I. Talmy, UHTCs: Ultra-High Temperature Ceramic Materials for Extreme Environment Applications, Electrochem. Soc. Interface 16[4] (2007) 30–36. doi: https://doi.org/10.1149/2.F04074IF.

[4] E.V. Clougherty, D. Kalish, E.T. Peters. Research and Development of Refractory Oxidation Resistant Diborides. Technical Report AFML- TR- 68- 190, ManLabs Incorporated, Wright Patterson Air Force Base, OH; 1968.

[5] J.J. Melendez-Martinez, A. Dominguez-Rodriguez, F. Monteverde, C. Melandri, G. de Portu, Characterization and high temperature mechanical properties of zirconium boride-based materials, J. Eur. Ceram. Soc. 22[14-15] 2002 2543–2549. doi: https://doi.org/10.1016/S0955-2219(02)00114-0.

[6] W.-W. Wu, Y. Sakka, M. Estili, T.S. Suzuki, T. Nishimura, G.-J. Zhang, Microstructure and high-temperature strength of textured and non-textured ZrB2 ceramics. Sci. Technol. Adv. Mater. 15[1] (2014) 014202. doi: 10.1088/1468-6996/15/1/014202.

[7] X.-G. Wang, W.-M. Guo, G.-J. Zhang, Pressureless sintering mechanism and microstructure of ZrB2–SiC ceramics doped with boron, Scr. Mater. 61 [2] (2009) 177–180. doi: https://doi.org/10.1016/j.scriptamat.2009.03.030.

[8] T.H. Squire, J. Marschall, Material property requirements for analysis and design of UHTC components in hypersonic applications, J. Eur. Ceram. Soc. 30[11] (2010) 2239–2251. doi: https://doi.org/10.1016/j.jeurceramsoc.2010.01.026.

[9] W.G. Fahrenholtz, G.E. Hilmas, Oxidation of ultra-high temperature transition metal diboride ceramics, Int. Mater. Rev. 57[1] (2012) 61–72. doi: https://doi.org/10.1179/1743280411Y.0000000012.

[10] A. Paul, D.D. Jayaseelan, S. Venugopal, E. Zapata-Solvas, J. Binner, B. Vaidhyanathan, A. Heaton, P. Brown, W.E. Lee, UHTS composites for hypersonic applications, Am. Ceram. Soc. Bull., 91[1] (2012), 22–29.

[11] S. Guo. T. Liu, D.-H. Ping, T. Nishimura, Enhanced high-temperature strength of HfB2–SiC composite up to 1600°C, J. Eur. Ceram. Soc. 38[4] (2018) 1152–1157. doi: https://doi.org/10.1016/j.jeurceramsoc.2017.12.040.

[12] A. Bellosi, F. Monteverde, D. Sciti, Fast densification of ultra-high temperature ceramics by spark plasma sintering, Int. J. Appl. Ceram. Technol. 3 (2006) 32–40. doi: https://doi.org/10.1111/j.1744-7402.2006.02060.x.

[13] E. Zapata-Solvas, D.D. Jayaseelan, H.T. Lin, P. Brown, W.E. Lee, Mechanical properties of ZrB2- and HfB2-based ultra-high temperature ceramics fabricated by spark plasma sintering, J. Eur. Ceram. Soc. 33[7] (2013) 1373–1386. doi: https://doi.org/10.1016/j.jeurceramsoc.2012.12.009.

[14] F. Monteverde, A. Bellosi, Microstructure and properties of an HfB2–SiC composite for ultra-high temperature applications, Adv. Eng. Mater. 6[5] (2004), 331–336. doi: https://doi.org/10.1002/adem.200400016.

[15] D. Demirskyi, T.S. Suzuki, S. Grasso, O. Vasylkiv, Microstructure and flexural strength of hafnium diboride via flash and conventional spark plasma sintering, J. Eur. Ceram. Soc. 39[4] (2019) 898–906. doi: https://doi.org/10.1016/j.jeurceramsoc.2018.12.012.

[16] L. Silvestroni, N. Gilli, A. Migliori, D. Sciti, J. Watts, G.E. Hilmas, W.G. Fahrenholtz, A simple route to fabricate strong boride hierarchical composites for use at ultra-high temperature, Compos. B. Eng. 183 (2020) 107618. doi: https://doi.org/10.1016/j.compositesb.2019.107618.

[17] J. Watts, G. Hilmas, W.G. Fahrenholtz, D. Brown, B. Clausen, Stress measurements in ZrB2–SiC composites using Raman spectroscopy and neutron diffraction, J. Eur. Ceram. Soc. 30 [11] (2010) 2165–2171. doi: https://doi.org/10.1016/j.jeurceramsoc.2010.02.014.

[18] D. Kalish, E.V. Clougherty, K. Kreder, Strength, fracture mode, and thermal stress resistance of HfB2 and ZrB2, J. Am. Ceram. Soc. 52[1] (1969), 30–36. doi: https://doi.org/10.1111/j.1151-2916.1969.tb12655.x.

[19] H.J. Brown-Shaklee, W.G. Fahrenholtz, G.E. Hilmas, Densification behavior and microstructure evolution of hot- pressed HfB2, J. Am. Ceram. Soc., 94[1] (2011) 49–58. doi: https://doi.org/doi/10.1111/j.1551-2916.2010.04063.x.

[20] E.W. Neuman, G.E. Hilmas, W.G. Fahrenholtz, Strength of zirconium diboride to 2300°C, J. Am. Ceram. Soc.96[1] (2013) 47–50. doi: https://doi.org/10.1111/jace.12114.

[21] A.C. Murchie, J.L. Watts, W.G. Fahrenhotlz, G.E. Hilmas, Mechanical properties of borothermally synthesized zirconium diboride at elevated temperatures, Int. J. Appl. Ceram. Technol. 18[4] (2021) 1235–1243. doi: https://doi.org/10.1111/ijac.13755.

[22] J.-X. Liu, G.-J. Zhang, F.-F. Xu, W.-W. Wu, H.-T. Liu, Y. Sakka, T. Nishimura, T.S. Suzuki, D.-W. Ni, J. Zou, Densification, microstructure evolution and mechanical properties of WC doped HfB2–SiC ceramics, J. Eur. Ceram. Soc. 35[10] (2015) 2707-2714. doi: https://doi.org/10.1016/j.jeurceramsoc.2015.04.009.

[23] S. Guo, In situ hot-pressed ZrB2-based composite with polycarbosilane-derived SiC - Microstructure and mechanical behavior, J. Am. Ceram. Soc., 102[6] (2019) 3286–3295. doi: https://doi.org/10.1111/jace.16248.

[24] J. Zou, G.-J. Zhang, C.-F. Hu, T. Nishimura, Y. Sakka, H. Tanaka, J. Vleugels, O. Van der Biest, High-temperature bending strength, internal friction and stiffness of ZrB2–20 vol% SiC ceramics, J. Eur. Ceram. Soc. 32[10] (2012) 2519–2527. doi: https://doi.org/10.1016/j.jeurceramsoc.2012.01.035.

[25] O.N. Grigoriev, A.V. Stepanenko, V.B. Vinokurov, I.P. Neshpor, T.V. Mosina, L. Silvestroni, ZrB2 – SiC ceramics: Residual stresses and mechanical properties, J.

Eur. Ceram. Soc. 41[9] (2021) 4720–4727. doi: https://doi.org/10.1016/j.jeurceramsoc.2021.02.053.

[26] P. Hu, Z. Wang, Flexural strength and fracture behavior of ZrB2–SiC ultra-high temperature ceramic composites at 1800°C, J. Eur. Ceram. Soc. 40[4] (2010) 1021–1026. doi: https://doi.org/10.1016/j.jeurceramsoc.2009.09.029.

[27] E.W. Neuman, G.E. Hilmas, WG. Fahrenholtz, Mechanical behavior of zirconium diboride–silicon carbide–boron carbide ceramics up to 2200 °C, J. Eur. Ceram. Soc. 35[2] (2015) 463–467. doi: https://doi.org/10.1016/j.jeurceramsoc.2014.09.021.

[28] D. Vedel, O. Grigoriev, P. Mazur, A. Osipov, M. Brodnikovskyi, L. Silvestroni, Effect of Mo2C addition on the mechanical properties and oxidation resistance of ZrB2-SiC ceramics, J. Alloys Compd. 879 (2021) 160398. doi: https://doi.org/10.1016/j.jallcom.2021.160398.

[29] D.V. Vedel, O.N. Grigoriev, P.V. Mazur, A.E. Osipov, Structure, Strength, and Oxidation Resistance of Ultrahigh-Temperature ZrB2–SiC–WC Ceramics, Powder Metall Met. Ceram. 60 (2021) 60–68. doi: https://doi.org/10.1007/s11106-021-00215-3.

[30] L.Silvestroni, H.-J. Kleebe, W.G. Fahrenholtz, J. Watts, Super-strong materials for temperatures exceeding 2000 °C, Sci Rep 7 (2017) 40730. doi: https://doi.org/10.1038/srep4073.

[31] W. Hao, N. Ni, Y. Guo, H. Cai, X. Fan, Y. Yao, X. Zhao, P. Xiao, Strong and tough HfC-HfB2 solid-solution composites obtained by reactive sintering with a SiB6 additive, Ceram. Int. 46 [10,B] (2020) 16257–16265. doi: https://doi.org/10.1016/j.ceramint.2020.03.182.

[32] J. Zou, G.-J. Zhang, Y.-M. Kan, T. Ohji, Pressureless sintering mechanisms and mechanical properties of hafnium diboride ceramics with pre-sintering heat

treatment, Scr. Mater. 62[3] (2010) 159–162. doi: https://doi.org/10.1016/j.scriptamat.2009.10.014.

[33] A. Carrasco-Pena, R. Jordan, J. Dieguez, A. Coronado-Rodríguez, V.B. Ozdemir, K. Kwok, N. Orlovskaya, D.A. Vazquez-Molina, F.J. Uribe-Romo, A. Bolon, M. Radovic, S. Grasso, and M.J. Reece, Design and development of ring-on-ring jig for biaxial strength testing of brittle ceramic composite materials: ZrB2-30wt-%SiB6, Adv. Appl. Ceram. 118[4] (2020) 159–168, doi: https://doi.org/10.1080/17436753.2019.1613102.

[34] W.G. Fahrenholtz, E.W. Neuman, H.J. Brown-Shaklee, G.E. Hilmas, Superhard Boride–Carbide Particulate Composites, J. Am. Ceram. Soc. 93[11] (2010) 3580–3583. doi: https://doi.org/10.1111/j.1551-2916.2010.04109.x.

[35] D. Demirskyi, O. Vasylkiv, Consolidation and grain growth of tantalum diboride during spark plasma sintering, Ceram. Int. 42 [14] (2016) 16396–16400. doi: https://doi.org/10.1016/j.ceramint.2016.07.059.

[36] D. Demirskyi, O. Vasylkiv, Hot-spots generation, exaggerated grain growth and mechanical performance of silicon carbide bulks consolidated by flash spark plasma sintering, J. Alloys Compd. 691 (2017) 466–473. doi: https://doi.org/10.1016/j.jallcom.2016.08.234.

[37] D. Demirskyi, O. Vasylkiv, Analysis of the high-temperature flexural strength behavior of B4C–TaB2 eutectic composites produced by in situ spark plasma sintering, Mater. Sci. Eng. A 697 (2017) 71–78. doi: https://doi.org/10.1016/j.msea.2017.04.093.

[38] D. Demirskyi, O. Vaslykiv, Spark plasma sintering and high-temperature strength of B6O–TaB2 ceramics, J. Eur. Ceram. Soc. 37[8] (2017) 3009–3014. doi: https://doi.org/10.1016/j.jeurceramsoc.2017.02.052.

[39] D. Demirskyi, I. Solodkyi, T. Nishimura, O. Vasylkiv, Fracture and property relationships in the double diboride ceramic composites by spark plasma sintering

of TiB2 and NbB2, J. Am. Ceram. Soc. 102[7] (2019) 4259–4271. doi: https://doi.org/10.1111/jace.16276.

[40] G.R. Anstis, P. Chantikul, B.R. Lawn, D.B. Marshall, A Critical Evaluation of Indentation Techniques for Measuring Fracture Toughness: I, Direct Crack Measurements, J. Am. Ceram. Soc. 64[9] (1981) 533–538. doi: https://doi.org/10.1111/j.1151-2916.1981.tb10320.x.

[41] D. Demirskyi, T.S. Suzuki, K. Yoshimi, O. Vasylliv, Consolidation and high-temperature strength of monolithic lanthanum hexaboride, J. Am. Ceram. Soc. (2022). doi: https://doi.org/10.1111/jace.18331.

[42] M. Vlasse, G.A. Slack, M. Garbauskas, J.S. Kasper, J.C. Viala, The crystal structure of SiB6, J. Solid State Chem. 63[1] (1986) 31–45. doi: https://doi.org/10.1016/0022-4596(86)90149-0.

[43] Telle R., Structure and properties of Si-doped boron carbide. In: R. Freer (ed), The Physics and Chemistry of Carbides, Nitrides and Borides. Kluwer Academic Publishers: Dordrecht, 1990, 249–267. doi: https://doi.org/10.1007/978-94-009-2101-6_16.

[44] Telle R., Sigl L.S. and Takagi K., Boride-based hard materials. In: ed. R. Riedel (ed), Handbook of Ceramic Hard Materials. vol. 2, Wiley-VCH, Weinheim, Germany, 2000, pp. 802–945. doi: https://doi.org/10.1002/9783527618217.ch22.

[45] H.-W. Ki,. Y.-H. Koh, H.-E. Kim, Kim Reaction sintering and mechanical properties of B4C with addition of ZrO2, J. Mater. Res. 15[11] (2000) 2431–2436. doi: https://doi.org/10.1557/JMR.2000.0349.

[46] A. Goldstein. Y. Geffen. A. Goldenberg, Boron Carbide-Zirconium Boride In Situ Composites by the Reactive Pressureless Sintering of Boron Carbide–Zirconia Mixtures, J. Am. Ceram. Soc. 84[3] (2001) 642–644. doi: https://doi.org/10.1111/j.1151-2916.2001.tb00714.x.

[47] S.C. Zhang, G.E. Hilmas, W.G. Fahrenholtz, Pressureless Densification of Zirconium Diboride with Boron Carbide Additions, J. Am. Ceram. Soc. 89[5] (2006) 1544–1550. doi: https://doi.org/10.1111/j.1551-2916.2006.00949.x.

[48] T.Ya. Kosolapova. Properties, synthesis and application of refractory compounds. Reference Book. Metallurgiya, Moscow, 1986. (in Russian).

[49] R.B. Kotelnikov, S.N. Bashlykov, Z.G. Galiakbarov, A.I. Kashtanov, Extra refractory elements and compounds, Metallurgiya, Moscow, 1968. (in Russian).

Part 3.2

[50] D. Demirskyi, H. Borodianska, Y. Sakka, O. Vasylkiv, Ultra-high elevated temperature strength of TiB2-based ceramics consolidated by spark plasma sintering, J. Eur. Ceram. Soc. 37 [1] (2017) 393–397.

[51] D. Demirskyi, Y. Sakka, In Situ Fabrication of B4C–NbB2 Eutectic Composites by Spark–Plasma Sintering, J. Am. Ceram. Soc. 97[8] (2014) 2376–2378. doi: https://doi.org/10.1111/jace.13083.

[52] https://crystdb.nims.go.jp.

[53] B. Morosin, G.H. Kwei, A.C. Lawson, T.L. Aselage, D. Emin, Neutron powder diffraction refinement of boron carbides nature of intericosahedral chains, J. Alloys Compd. 226 [1–2] (1995) 121–125. doi: https://doi.org/10.1016/0925-8388(95)01585-X.

[54] L. Bsenko, T. Lundstrom, The high-temperature hardness of ZrB2 and HfB2, J. Less Common Met. 34 [2] (1974) 273–278. doi: https://doi.org/10.1016/0022-5088(74)90169-6.

[55] R. Tu, N. Li, Q. Li, S. Zhang, L. Zhang, T. Goto, Microstructure and mechanical properties of B4C–HfB2–SiC ternary eutectic composites prepared by arc melting, J. Eur. Ceram. Soc. 36[4] (2016) 959–966. doi: https://doi.org/10.1016/j.jeurceramsoc.2015.11.044.

[56] S.S. Ordan'yan, A.I. Dmitriev, Interaction in the system B4C–HfB2, Powder Metall. Met. Ceram., 28[5] (1989) 424–426. doi: https://doi.org/10.1007/BF00795052.

[57] S.S. Ordan’yan, Interaction regularities in SiC–MeIV–VIB2 systems, Zh. Prikl. Khim. 66 [11] (1993) 2439–2444.

[58] D.R. Secrist, Phase Equilibria in the System Boron Carbide-Silicon Carbide, J. Am. Ceram. Soc. 47[3] (1964) 127–130. doi: https://doi.org/10.1111/j.1151-2916.1964.tb14369.x.

[59] S.S. Ordan'yan, D.D. Nesmelov, D.P. Danilovich, Yu.P. Udalov, SiC–B4C–MedB2 systems and the prospects for creating composite ceramic materials based on them, Izv. vuzov. Poroshk. metallurgiya i funkts. pokrytiya, 4 (2016) 41–50. [In Russian]. doi: https://dx.doi.org/10.17073/1997-308X-2016-4-41-50.

[60] R. Tu, D. Zheng, Q. Sun, M. Han, et al., Ultra-Fast Fabrication of <110>-Oriented β-SiC Wafers by Halide CVD, J. Am. Ceram. Soc. 99[1] (2016) 84–88. doi: https://doi.org/10.1111/jace.13980.

[61] H. Kikuchi, R.K. Kalia, A. Nakano, P. Vashishta, P.S. Branicio, F. Shimojo, Brittle Dynamic Fracture of Crystalline Cubic Silicon Carbide (3C-SiC) via Molecular Dynamics Simulation, J. Appl. Phys., 98 [10] (2005) 103524. doi: https://doi.org/10.1063/1.2135896.

[62] E.K.K. Abavare, J.I. Iwata, A. Oshiyama, Atomic Reconstruction and Electron States at Interfaces Between 3C-SiC(111) and Si(110), Phys. Rev. B, 87 [23] (2013) 235321. doi: https://doi.org/10.1103/PhysRevB.87.235321.

[63] T. Nishiguchi, M. Nakamura, K. Nishio, T. Isshiki, S. Nishino, Heteropitaxial Growth of (111) 3C-SiC on Well-Lattice-Mathced (110) Si Substrates by Chemical Vapor Deposition, Appl. Phys. Lett., 84 [16] (2004) 3082–3084. doi: https://doi.org/10.1063/1.1719270.

[64] M Anderson, J. Gebbie-Rayet, A Hill et al., Predicting crystal growth via a unified kinetic three-dimensional partition model, Nature 544 (2017) 456–459. doi: https://doi.org/10.1038/nature21684.

[65] P.M. Sargent, M.F. Ashby, Deformation-mechanism maps for silicon carbide, Scripta Met., 17[7] (1983) 951–957. doi: https://doi.org/10.1016/0036-9748(83)90269-7.

[66] A. Stukowski, Visualization and analysis of atomistic simulation data with OVITO–the Open Visualization Tool, Modelling Simul. Mater. Sci. Eng., 18 (2010) 015012. doi: https://doi.org/10.1088/0965-0393/18/1/015012.

[67] J.-M. Bind, Phase transformation during hot-pressing of cubic SiC, Mater. Res. Bull. 13[2] (1978) 91–96. doi: https://doi.org/10.1016/0025-5408(78)90071-5.

[68] A. Lipp, M. Roder, Verbindungen im System B-C-Si bzw. B-Si, Z. Anorg. Allg. Chem. 334 [5-6] (1966) 225–229. doi: https://doi.org/10.1002/zaac.19663440502.

[69] F. Ye, Z. Hou, H. Zhang, L. Liu, Densification and Mechanical Properties of Spark Plasma Sintered B4C with Si as a Sintering Aid, J. Am. Ceram. Soc. 93[10] (2010) 2956–2959. doi: https://doi.org/10.1111/j.1551-2916.2010.03931.x.

[70] K. Sariam, J.K. Sobner, T.S.R.Ch Murthy, R.C. Hubli, A.K. Suri, Development of B4C–HfB2 composites by reaction hot pressing, Int. J. Refract. Hard Met. 35 (2012) 32–40. doi: https://doi.org/10.1016/j.ijrmhm.2012.03.004.

[71] F. Thevenot, Boron carbide - a comprehensive review. J. Eur. Ceram. Soc. 6[4] (1990) 205–225. doi: https://doi.org/10.1016/0955-2219(90)90048-K.

[72] N. Cho, Z. Bao, R.F. Speyer, Density- and Hardness-optimized Pressureless Sintered and Post-hot Isostatic Pressed B4C, J. Mater. Res. 10 [8] (2005) 2110–2116 doi: https://doi.org/10.1557/JMR.2005.0260.

[73] H. Probst, W. Sanders, High Temperature Mechanical Properties of Polycrystalline Hafnium Carbide and Hafnium Carbide Containing 13-Volume-Percent Hafnium Diboride (1969), Lewis Research Center, Cleveland, Ohio.

[74] F. Garofalo. Fundamentals of creep and creep-rupture in metals, MacMillan, New York NY, 1965.

Figure captions

Figure 1. Microstructure of the SPSed SiB_6 ceramic after consolidation at 1900°C using a Ta-foil. The volume fraction of the SiC clusters using Fiji was 4.6±0.3 vol.%. (a) was obtained in the SE mode, (b) was obtained in the BSE mode. Light-gray phases in (b) are due to the grain pull-outs. Insets in (a) and (b) provide typical EDX for the $B_{13}(Si,B,C)_2$ and SiC phases, respectively. (c) illustrates how Ta-foil was used during the SPS process: reaction between tantalum foil and graphite foil produces the ~30 μm thick TaC layer (see ref. [41] for details).

Figure 2. Observed and refined X-ray diffraction pattern of the SiB_6 after SPS at 1900 °C. Vertical lines show the Bragg peak positions for the refined phases. The lattice parameters for the $B_{13}C_2$ phase are a = 5.58 Å and c = 12.25 Å.

Figure 3. X-ray diffraction pattern of the raw SiB_6 powder. Silicon was used as an external standard. All other peaks belong to silicon hexaboride. The vertical lines show the Bragg peak positions for the SiB_6 phase. The lattice parameters for the SiB_6 phase (space group #58, *Pnnm*) are a = 14.42 Å, b = 18.30 Å and c = 9.89 Å.

Figure 4. Microstructure of the SiB_6 ceramic after SPS at 1900 °C. Powders were consolidated using a 'regular' SPS packaging (see inset), which involves only graphite foil. The thickness for such foil is ~1 mm. Top two millimeters was removed during polishing. The volume fraction of the SiC clusters using Fiji was 5.1±0.4 vol.%. The graphite clusters (medium-gray color) occupied 6.2±0.2 vol.%.

Figure 5. Shrinkage curve of the HfB_2–SiB_6 composite during spark plasma sintering at 1900 °C.

Figure 6. Observed and refined X-ray diffraction pattern of the HfB_2–SiB_6 ceramics after SPS. Inset shows position of the most intensive peaks of the $B_{12}(C,Si,B)_3$ phase on a logarithmic scale. The lattice parameters for the $B_{12}(C,Si,B)_3$ phase are a = 5.60(7) Å, and c = 12.15 Å. The Bragg peak positions for HfB_2 and $B_{12}(C,Si,B)_3$ are indicated by the green and violet vertical markers, respectively.

Figure 7. Microstructure of the HfB_2–SiB_6 ceramic SPSed at 1900 °C in the vicinity of the pseudo-eutectic aggregate. (b) shows the enlarged area of the $B_{12}(C,Si,B)_3$–SiC area. The crack in the SiC phase here originated from the indent by the load of 98 N. Inset in (b) shows typical B_4C–SiC eutectic structures prepared as parallel experiment using the SPS method with the 75 B_4C:25 SiC vol.%. The maximum shrinkage rate indicating the eutectic formation as in [51] during the SPS of the B_4C–SiC eutectic was 2085±10°C.

Figure 8. Illustration of the surface during the crystal growth process for cubic silicon carbide at (a) 1900 °C and (b) 1000 °C. (c) shows typical B_4C–SiC eutectic structure.

Figure 9. SEM micrographs of HfB_2-SiB_6 ceramics consolidated using the spark plasma method. Pale-gray phase is hafnium diboride, while the dark black is the Si-rich boron carbide phase. Light-gray phase was identified as silicon carbide. (a)–(c) contain EDX data from the spot analysis.

Figure 10. Silicon content for the $B_{13}(Si,B,C)_2$ as detected by the EDX analysis performed on the polished surfaces of the SPSed HfB_2–SiB_6 composite. Right image shows a distribution frequency of Si content in the $B_{13}(Si,B,C)_2$.

Figure 11. Force-displacement curve recorded during the fracture toughness evaluation using the single edge notched beam flexural test at room temperature.

Figure 12. Effect of temperature and composition on the flexural strength of HfB_2-based ceramics [4, 11, 14–16]. Strength of 'as sintered' ceramic reported from ref. [16], and its corresponding test at 1500 °C was performed in air.

Figure 13. Typical strain-stress curves during flexural tests at 25°C, 1600°C and 1800°C.

Figure 14. Representative microstructures of the HfB_2–SiB_6 ceramics. (a) polished, (b) fractured at room temperature, (c) fractured at 1600 °C, (d–f) fractured at 1800 °C. (e and f) taken in the SE mode. (a–d) were obtained in the BSE mode. (c,d)

were tested in argon, while (e,f) were tested in nitrogen. In (f) a quasi-layered fracture was observed.

Tables

Table 1. Composition of binary and ternary eutectics in the HfB_2–B_4C–SiC system

System	Concentration in mol.%			Concentration in vol.%			Melting point, °C	Reference
	HfB_2	B_4C	SiC	HfB_2	B_4C	SiC		
HfB_2-B_4C-SiC	15	45	40	16	56	28	-	[55]
HfB_2-B_4C	22	78	-	20	80	-	2380±30	[56]
HfB_2-SiC	22	-	78	30	-	70	2360±20	[57]
B_4C-SiC	-	64	36	-	76	24	2300	[58]
B_4C-SiC	-	58	42	-	71	29	2150	[59]
$B_{12}(C,Si,B)_3$-SiC clusters	-	-	-	-	82±6	18±6	-	This study, SEM
HfB_2-$B_{12}(C,Si,B)_3$-SiC*	-	-	-	74.5±1.8†	23.3±2.6†	2.2±1.1†	-	This study, SEM
HfB_2-$B_{12}(C,Si,B)_3$-SiC*	-	-	-	72	28	-	-	This study, XRD

*Initial ratio HfB_2:SiB_6 80:20 vol.%.

† Median value and the standard deviation using multiple SEM images.

Figure captions

Figure 1. Microstructure of the SPSed SiB_6 ceramic after consolidation at 1900°C using a Ta-foil. The volume fraction of the SiC clusters using Fiji was 4.6±0.3 vol.%. (a) was obtained in the SE mode, (b) was obtained in the BSE mode. Light-gray phases in (b) are due to the grain pull-outs. Insets in (a) and (b) provide typical EDX for the $B_{13}(Si,B,C)_2$ and SiC phases, respectively. (c) illustrates how Ta-foil was used during the SPS process: reaction between tantalum foil and graphite foil produces the ~30 μm thick TaC layer (see ref. [41] for details).

Figure 2. Observed and refined X-ray diffraction pattern of the SiB_6 after SPS at 1900 °C. Vertical lines show the Bragg peak positions for the refined phases. The lattice parameters for the $B_{13}C_2$ phase are a = 5.58 Å and c = 12.25 Å.

Figure 3. X-ray diffraction pattern of the raw SiB_6 powder. Silicon was used as an external standard. All other peaks belong to silicon hexaboride. The vertical lines show the Bragg peak positions for the SiB_6 phase. The lattice parameters for the SiB_6 phase (space group #58, *Pnnm*) are a = 14.42 Å, b = 18.30 Å and c = 9.89 Å.

Figure 4. Microstructure of the SiB_6 ceramic after SPS at 1900 °C. Powders were consolidated using a 'regular' SPS packaging (see inset), which involves only graphite foil. The thickness for such foil is ~1 mm. Top two millimeters was removed during polishing. The volume fraction of the SiC clusters using Fiji was 5.1±0.4 vol.%. The graphite clusters (medium-gray color) occupied 6.2±0.2 vol.%.

Figure 5. Shrinkage curve of the HfB_2–SiB_6 composite during spark plasma sintering at 1900 °C.

Figure 6. Observed and refined X-ray diffraction pattern of the HfB_2–SiB_6 ceramics after SPS. Inset shows position of the most intensive peaks of the $B_{12}(C,Si,B)_3$ phase on a logarithmic scale. The lattice parameters for the $B_{12}(C,Si,B)_3$ phase are a = 5.60(7) Å, and c = 12.15 Å. The Bragg peak positions for HfB_2 and $B_{12}(C,Si,B)_3$ are indicated by the green and violet vertical markers, respectively.

Figure 7. Microstructure of the HfB_2–SiB_6 ceramic SPSed at 1900 °C in the vicinity of the pseudo-eutectic aggregate. (b) shows the enlarged area of the $B_{12}(C,Si,B)_3$–SiC area. The crack in the SiC phase here originated from the indent by the load of 98 N. Inset in (b) shows typical B_4C–SiC eutectic structures prepared as parallel experiment using the SPS method with the 75 B_4C:25 SiC vol.%. The maximum shrinkage rate indicating the eutectic formation as in [51] during the SPS of the B_4C–SiC eutectic was 2085±10°C.

Figure 8. Illustration of the surface during the crystal growth process for cubic silicon carbide at (a) 1900 °C and (b) 1000 °C. (c) shows typical B_4C–SiC eutectic structure.

Figure 9. SEM micrographs of HfB_2-SiB_6 ceramics consolidated using the spark plasma method. Pale-gray phase is hafnium diboride, while the dark black is the Si-rich boron carbide phase. Light-gray phase was identified as silicon carbide. (a)–(c) contain EDX data from the spot analysis.

Figure 10. Silicon content for the $B_{13}(Si,B,C)_2$ as detected by the EDX analysis performed on the polished surfaces of the SPSed HfB_2–SiB_6 composite. Right image shows a distribution frequency of Si content in the $B_{13}(Si,B,C)_2$.

Figure 11. Force-displacement curve recorded during the fracture toughness evaluation using the single edge notched beam flexural test at room temperature.

Figure 12. Effect of temperature and composition on the flexural strength of HfB_2-based ceramics [4, 11, 14–16]. Strength of 'as sintered' ceramic reported from ref. [16], and its corresponding test at 1500 °C was performed in air.

Figure 13. Typical strain-stress curves during flexural tests at 25°C, 1600°C and 1800°C.

Figure 14. Representative microstructures of the HfB_2–SiB_6 ceramics. (a) polished, (b) fractured at room temperature, (c) fractured at 1600 °C, (d–f) fractured at 1800 °C. (e and f) taken in the SE mode. (a–d) were obtained in the BSE mode. (c,d)

were tested in argon, while (e,f) were tested in nitrogen. In (f) a quasi-layered fracture was observed.

Declaration of interests

☒ The authors declare that they have no known competing financial interests or personal relationships that could have appeared to influence the work reported in this paper.

☐The authors declare the following financial interests/personal relationships which may be considered as potential competing interests:

Video1

Video2

Video3

Click here to access/download

Supplementary Information

Video3.mp4